AIP | The Journal of Chemical Physics

Three-dimensional kinetic Monte Carlo simulations of diamond chemical vapor deposition

W. J. Rodgers, P. W. May, N. L. Allan, and J. N. Harvey

Citation: The Journal of Chemical Physics **142**, 214707 (2015); doi: 10.1063/1.4921540
View online: http://dx.doi.org/10.1063/1.4921540
View Table of Contents: http://scitation.aip.org/content/aip/journal/jcp/142/21?ver=pdfcov
Published by the AIP Publishing

Articles you may be interested in

Simulations of chemical vapor deposition diamond film growth using a kinetic Monte Carlo model and two-dimensional models of microwave plasma and hot filament chemical vapor deposition reactors
J. Appl. Phys. **108**, 114909 (2010); 10.1063/1.3516498

Simulations of chemical vapor deposition diamond film growth using a kinetic Monte Carlo model
J. Appl. Phys. **108**, 014905 (2010); 10.1063/1.3437647

Morphology and bonding states of chemical vapor deposition diamond films nucleation surface
Appl. Phys. Lett. **96**, 104101 (2010); 10.1063/1.3352108

Study of the early stage of SiO 2 growth by a TEOS–O 2 plasma mixture using a three-dimensional Monte Carlo model
J. Vac. Sci. Technol. A **19**, 743 (2001); 10.1116/1.1362676

Postnucleation surface transport-kinetical phenomena and morphological instability in film deposition from vapor
J. Appl. Phys. **89**, 2151 (2001); 10.1063/1.1339209

Reuse of AIP Publishing content is subject to the terms: https://publishing.aip.org/authors/rights-and-permissions. Downloaded to IP: 134.58.253.57 On: Tue, 19 Apr 2016 09:12:27

Three-dimensional kinetic Monte Carlo simulations of diamond chemical vapor deposition

W. J. Rodgers, P. W. May,[a] N. L. Allan, and J. N. Harvey
School of Chemistry, University of Bristol, Bristol BS8 1TS, United Kingdom

(Received 4 March 2015; accepted 7 May 2015; published online 4 June 2015)

A three-dimensional kinetic Monte Carlo model has been developed to simulate the chemical vapor deposition of a diamond (100) surface under conditions used to grow single-crystal diamond (SCD), microcrystalline diamond (MCD), nanocrystalline diamond (NCD), and ultrananocrystalline diamond (UNCD) films. The model includes adsorption of CH_x (x = 0, 3) species, insertion of CH_y (y = 0-2) into surface dimer bonds, etching/desorption of both transient adsorbed species and lattice sidewalls, lattice incorporation, and surface migration but not defect formation or renucleation processes. A value of ~200 kJ mol^{-1} for the activation Gibbs energy, $\Delta G^{\ddagger}_{\text{etch}}$, for etching an adsorbed CH_x species reproduces the experimental growth rate accurately. SCD and MCD growths are dominated by migration and step-edge growth, whereas in NCD and UNCD growths, migration is less and species nucleate where they land. Etching of species from the lattice sidewalls has been modelled as a function of geometry and the number of bonded neighbors of each species. Choice of appropriate parameters for the relative decrease in etch rate as a function of number of neighbors allows flat-bottomed etch pits and/or sharp-pointed etch pits to be simulated, which resemble those seen when etching diamond in H_2 or O_2 atmospheres. Simulation of surface defects using unetchable, immobile species reproduces other observed growth phenomena, such as needles and hillocks. The critical nucleus for new layer growth is 2 adjacent surface carbons, irrespective of the growth regime. We conclude that twinning and formation of multiple grains rather than pristine single-crystals may be a result of misoriented growth islands merging, with each island forming a grain, rather than renucleation caused by an adsorbing defect species. © *2015 Author(s). All article content, except where otherwise noted, is licensed under a Creative Commons Attribution 3.0 Unported License.* [http://dx.doi.org/10.1063/1.4921540]

I. INTRODUCTION

The chemical vapor deposition (CVD) of diamond is now well-developed with many existing and potential commercial applications in electronics, mechanical parts/tools, sensors, and optics.[1] The CVD process involves a low pressure reactor into which a small amount of a hydrocarbon gas (usually CH_4) and molecular hydrogen (H_2) is introduced. The ratio is typically 1%-5% CH_4 in H_2 with inert gases such as N_2 and Ar also sometimes included. The composition of the process gas mixture and other parameters such as substrate temperature, pressure, and temperature of the reacting gas determines the ultimate structure and quality of the diamond.[2] The CVD process usually produces polycrystalline diamond with grain sizes from 10 nm to 1 mm. The resulting diamond films are loosely classified depending upon their crystallite size: grain sizes from 4 nm to ~10 nm are termed ultrananocrystalline diamond (UNCD), 10-200 nm nanocrystalline diamond (NCD), and from ~200 nm to 100 μm microcrystalline diamond (MCD). Larger sizes are considered single-crystal diamond (SCD).

Control over both morphology and specific electronic and mechanical properties requires detailed knowledge of the growth process, including the effects of the substrate temperature, gas composition, and process pressure. A "standard growth mechanism"[3] developed over twenty years ago is useful, but fails to fully account for the growth rate, the crystal size of polycrystalline films, and many other features observed experimentally. In this standard model, atomic H created by thermal or electron-impact dissociation of H_2 drives the process. The main growth species is the CH_3 radical.[4–6] This adds to radical sites (dangling bonds) on the diamond surface following hydrogen abstraction by atomic H. The fraction of surface radical sites, typically ~10%, depends upon the dynamic equilibrium between H-abstraction and H-addition reactions and thus the process conditions, such as the concentration of gas-phase atomic H just above the surface, $[H]_s$, and the substrate temperature, T_s. Most experimental and theoretical studies of diamond growth focus on the (100) surface of diamond, as growth leads to fewer defects than on other surfaces, such as (111) or (110), and can produce large, flat terraces of near perfect crystallinity under appropriate conditions. However, the (100) surface itself is known to reconstruct to hydrogen-terminated (2 × 1) dimer rows, henceforth referred to as the (100) – (2 × 1):H diamond surface, which needs to be considered in any model.

Because the substrate temperature is high (T_s > 700 °C), chemisorbed species such as CH_2 can migrate along or across a dimer row provided they have an adjacent radical site into

[a]Author to whom correspondence should be addressed. Electronic mail: paul.may@bristol.ac.uk

 © Author(s) 2015

Reuse of AIP Publishing content is subject to the terms: https://publishing.aip.org/authors/rights-and-permissions. Downloaded to IP: 134.58.253.57 On: Tue, 19 Apr 2016 09:12:27

which to move. The migration process is actually a complex chain of steps,[4] but because the radical sites are created by H-abstraction, the migration rate depends upon the local atomic H concentration. Adsorbed carbon species may migrate across the surface until they meet a step-edge, where they can become a permanent attachment to the diamond lattice (step-flow growth[7]), or they may be etched or desorbed back into the gas phase. Atomic H also plays an important role in determining the quality of the growing diamond film as well as catalysing migration. H atoms can etch graphitic or sp^2 carbon many times more rapidly than diamond-like sp^3 carbon,[8] and thus, the H-atom flux onto the surface continuously etches away any non-diamond carbon while generally leaving sp^3 carbon behind. Nevertheless, the etch rate of surface sp^3 hydrocarbon species is non-zero and varies with local environment. Indeed, studies using pure H_2 gas but under otherwise similar conditions to those used for diamond CVD show that the etch rate of (100) diamond is <10 nm h^{-1}.[9] However, this value is somewhat misleading as the etching occurs at defects, usually dislocations on the surface, which etch back laterally to form shallow rectangular etch pits.[10–12] Indeed, counting etch pits is often used as a method to determine the number density and distribution of dislocations at a diamond surface.[13] These observations all support the idea that isolated sp^3 hydrocarbon species on flat diamond terraces are etched away faster than those adjacent to a step-edge,[8] so hydrocarbon species preferentially reside and accumulate at step-edges. This "preferential etching"[14] is an alternative explanation for apparent step-edge growth.

Our group recently developed a modified version of the standard growth model which allows for incorporation of all the C_1 hydrocarbon radicals CH_3, CH_2, CH, and C atoms on both monoradical and biradical sites on the (100) diamond surface.[15] The inclusion of migration of CH_2 groups along and across the reconstructed dimer rows led to predicted growth rates within a factor of two of experiment, and average grain sizes for polycrystalline films that are also in good agreement, ranging from a few nm (UNCD) to mm (MCD and SCD). This growth model was then used as the basis for kinetic Monte Carlo (KMC) simulations of diamond growth.[16–23] Such simulations are based on a model diamond (usually (100)) surface and a set of all relevant processes, such as adsorption, etching/desorption, migration, and so on, and at each step of the simulation, a process is chosen with a probability proportional to its rate. Over the past 15 years, these KMC simulations have gradually become more sophisticated as the gas-phase and gas-surface chemical processes have become better understood. A review of all the KMC simulations by ourselves and other groups is given in our previous paper,[17] so for brevity, here, we shall only discuss briefly the two models from other groups that have been the most successful in reproducing experimental observations of diamond growth. In 1999-2000, Grujicic and Lai developed a multi-length-scale model of a diamond growth process which combined a reactor-scale and an atomic-scale model.[21–23] They used a full 3D model for diamond (111) and (100) surfaces, and a database of 12 gas-surface reactions, together with calculations for the flux of reactive species striking the surface, to produce a KMC model which had remarkable predictive power. Predicted aspects of diamond growth such as the temperature dependence of growth, the quality of the deposited film as judged by the concentration of point defects (vacancies and hydrogen atoms embedded in the film) and by surface roughness, as well growth rates, were all consistent with experiment. However, the simulation did not include surface migration, which is crucial in determining film growth and morphology. It also used the one-dimensional computer codes *Chemkin*/*SPIN* to estimate species concentrations above the growing surface. However, these codes cannot accurately simulate the transport and reactions occurring in a three-dimensional CVD chamber and also do not take into account the boundary conditions in the stagnation layer above the growth surface. As a result, the gas concentrations at the diamond surface (particularly those for atomic H) were overestimated by perhaps a factor of ~10-100. Also, reactions of C_2H_y species with the diamond were included as important growth processes, whereas we now know that these species have almost negligible concentration at the surface as a result of gas-phase reactions with atomic H.

More recently, another sophisticated KMC implementation was reported by Netto and Frenklach,[16] which used methyl radicals as the only growth species, with the incorporation into the diamond surface described by means of a ring-opening/closing mechanism. CH_2 migration along and across the dimer reconstructions was included, as well as the reforming of dimer-reconstructed bonds from two suitable adjacent surface radical sites. Etching was only considered to occur at isolated incorporated CH_2 groups and reconstructed dimers. The energetics and kinetic data for these reactions were sourced from numerous calculations and experimental measurements. Overall, their simulations showed that CH_3 can randomly adsorb upon a diamond surface and then migrate until multiple species coalesce. During this process, the substrate surface can act as a template for migrating species to form new dimer reconstructions and, in combination with etching, results in the smooth surface growth observed.

In our previous work to date,[18–20] the model was only two-dimensional (2D), i.e., translation along one horizontal axis ($\pm x$) plus vertical height, z (film thickness). The interplay between adsorption, etching/desorption, surface migration, and addition to the lattice was modelled using the most accurate values for gas concentrations and process conditions available from experiment or *ab initio* calculations. The rate of etching of adsorbed CH_2 species was set to one-tenth of the rate of adsorption based on the observed etch rates of SCD in H_2 microwave plasmas, even though the presence of shallow rectangular etch pits 100's of μm wide[8,24,25] suggests much faster lateral than vertical etching. Detailed *ab initio* calculations[26] showed that migration down a step-edge had a similar energy barrier to migration on the flat, and thus, migration down steps (the "lemmings" scenario[19]) is facile.

The main findings of the 2D model were that the average surface diffusion length, ℓ, is a key parameter controlling surface morphology. When $\ell < 2$, surface migration is limited by the lack of availability of surface radical sites, and the migrating surface species simply hop back and forth between two adjacent sites but do not travel far beyond their initial adsorption site. Thus, Eley–Rideal (ER) processes (i.e.,

Reuse of AIP Publishing content is subject to the terms: https://publishing.aip.org/authors/rights-and-permissions. Downloaded to IP: 134.58.253.57 On: Tue, 19 Apr 2016 09:12:27

direct adsorption from the gas phase) dominate the growth, leading to the rough surfaces seen in NCD and UNCD. Conversely, when migration occurs over greater distances $\ell > 2$, Langmuir–Hinshelwood (LH) processes dominate the growth producing the smoother surfaces of MCD and SCD. The model showed that β-scission processes were unimportant for MCD and SCD growth conditions, but removed up to 5% of the adsorbing carbon for NCD and UNCD growths. A simple model for insertion reactions was included in the model which showed that C_1H_x insertion reactions contributed ~1% to the growth for nearly all conditions, while C_2H_x ($x < 2$) insertion reactions are negligible due to their very low concentrations at the surface.

Despite these promising results, a 2D model for the diamond surface had a number of limitations in its predictive power. Geometrical effects on the surface, such as kinks in step-edges, recesses, and the shape of islands, could not be simulated. Indeed, the ultimate goal of being able to predict the morphology of diamond crystals as they evolve during the growth is impossible in only two dimensions.

II. THE NEW 3D KMC MODEL

In this paper, we now report a three-dimensional KMC model, with the surface being represented by a plane in the x and y directions, and growth occurring, as before, in the z-direction. In the 3D model, the initial (100) surface is now defined by an arbitrarily sized $N \times N \times M$ cubic grid which represents the diamond (100) surface in the x, y plane and height M with a nominally (100) – (2 × 1):H surface reconstruction, although this reconstruction is not explicitly modelled. The initial value of M was usually 1 for modelling growth but was set to typically 10 when simulating pure etching to allow many layers to etch away. Hydrocarbon species that adsorb onto this surface are treated as a $1 \times 1 \times 1$ block, which may migrate around the surface in the x and y directions, be etched away, or meet and add to an existing sidewall so propagating the next layer of growth. This 3D cubic grid model is clearly less realistic than the full 3D diamond structures adopted by Grujicic and Lai[21] and Netto and Frenklach[16] in their previous KMC simulations. However, the simplified geometry allows for extremely fast calculations and thus the simulation of growth of dozens of layers of diamond over large areas ($N \times N$ can be as large as 80×80) in manageable computation time.

Under most CVD diamond conditions, surface radical migrations and surface H abstraction/addition reactions have rates that are many thousands of times faster than the other processes being considered. If calculated explicitly, the code would waste most of its time repeatedly calculating these fast processes, even though they do not directly contribute to etching or growth. Instead, to speed up the calculation, an equilibrium approximation ("superbasin approach") is adopted, whereby the distribution of radical sites on the surface is randomized after each carbon addition, etch or migration process, whilst keeping the overall fraction of surface monoradicals, F_{mr}, constant. The value of F_{mr} was calculated based on the input values of [H], [H_2], and the gas and surface temperatures using the equation in Ref. 15.

To visualize the simulation, after each step involving movement of a species, the coordinates of all the surface blocks were saved in "xyz format" commonly used for 3D chemical structure modelling. Thus, the file could be loaded into suitable visualisation software (such as *Ovito*[27]) and viewed frame-by-frame or as a continuous movie.

A. Adsorption

Six distinct molecular species are considered: a hydrogen-terminated surface-carbon (–C_d–H), a radical surface-carbon (–$C_d^\bullet$), an adsorbed methyl (–C_d–CH_3), and three different adsorbed hydrocarbon radical species (–C_d–$CH_x^\bullet$ (x = 0-2)), where C_d represents a carbon atom bound on the surface of the diamond lattice and the dot ($^\bullet$) a "dangling bond." Table I lists the reactions these species can undergo, along with their rates.

Any of four gas-phase molecular species, C_1H_x (x = 0-3), can add to activated surface sites on the diamond lattice, decided at random. Of these species, the methyl radical CH_3 is the most important due to its much higher concentration in the vicinity of the surface.[28] We have used the previously calculated gas concentrations near the surface for different diamond deposition conditions: SCD, MCD, NCD, and UNCD (Table I in Ref. 20). For adsorption, a molecular species near the surface with a known mean velocity (calculated from the gas temperature and pressure) collides with the surface with a certain rate, and a sticking probability determines the probability of an adsorption event occurring (see Table I, process (d)).

Competing with adsorption processes is the direct insertion into surface C–C bonds by CH_x (x = 0-2) radicals. There is now a more detailed treatment of this than in our earlier work. The rate constants for these reactions have now been estimated using *ab initio* calculations[20,24] and are given in Table II, Eqs. (12a)–(12c). Although insertion reactions can occur at every surface site (not just the activated ones), due to the low concentrations of these radicals near the surface, the rates for these insertion processes are relatively small, typically <1% that for CH_3 addition to surface radicals, but non-negligible under some conditions. Higher hydrocarbons, such as C_2H_x species, have extremely low concentrations at the growth surface, and thus, negligible insertion rates, and these species have therefore not been included in the model.

B. Etching/desorption of surface species

In previous models of etching, the rate constant, k_{etch}, for etching isolated adspecies was initially considered to adopt a value based on an Arrhenius law with a pre-exponential factor equivalent to the collision frequency (assumed to be $\sim 10^{13}$ s^{-1}) and activation barrier, $\Delta G^{\ddagger}_{etch}$, equivalent to the C–C bond energy (348 kJ mol^{-1}). However, this gave an etch rate of almost zero, which is inconsistent with experiment. To correct this, an empirical value for k_{etch} was instead chosen based on the observation that the total etch rate from a diamond surface in the absence of gas-phase CH_4 is ~10% that of the growth rate when CH_4 is added (Eq. (9) in Table II).

For the new 3D model, to put the etching/desorption of sp^3-bonded carbon from the diamond lattice (Table I,

Reuse of AIP Publishing content is subject to the terms: https://publishing.aip.org/authors/rights-and-permissions. Downloaded to IP: 134.58.253.57 On: Tue, 19 Apr 2016 09:12:27

TABLE I. Reactions for each process included in model and their associated rate constants. Details of rate constants are found in Table II. C_d represents a carbon bonded into the diamond surface and • represents a radical site.

Process	Reaction	Rate constant
(a) Surface activation	(i) $H(g) + HC_d–C_dH \rightarrow {}^\bullet C_d–C_dH + H_2(g)$ (ii) $HC_d–C_dH \rightarrow {}^\bullet C_d–C_dH + H(g)$	$k_{activate}$
Adspecies activation	(i) $H(g) + CH_{x(1-3)}–C_d–C_dH \rightarrow {}^\bullet CH_{x(0-2)}–C_d–C_dH + H_2(g)$ (ii) $CH_{x(1-3)}–C_d–C_dH \rightarrow {}^\bullet CH_{x(0-2)}–C_d–C_dH + H(g)$	
(b) Surface deactivation	(i) $H_2(g) + {}^\bullet C_d–C_dH \rightarrow H(g) + HC_d–C_dH_d$ (ii) $H^\bullet(g) + {}^\bullet C_d–C_dH \rightarrow HC_d–C_dH_d$	$k_{deactivate}$
Adspecies deactivation	(i) $H_2(g) + {}^\bullet CH_{x(0-2)}–C_d–C_dH \rightarrow H(g) + CH_{x(1-3)}–C_d–C_dH$ (ii) $H^\bullet(g) + {}^\bullet CH_{x(0-2)}–C_d–C_dH \rightarrow CH_{x(1-3)}–C_d–C_dH$	
(c) CH_2/CH_3 etch	$H(g) + {}^\bullet CH_2–C_d–C_dH \rightarrow CH_4(g) + {}^\bullet Cd–Cd_H$	k_{etch}
(d) CH_x add	$CH_x(g) + {}^\bullet C_d–C_dH \rightarrow {}^\bullet CH_x–C_d–C_dH$	$k_{CHx-add}$
(e) Migration in 4 directions	$H–C_d–CH_2–C_d–H\ldots{}^\bullet C_d–C_d–H \rightarrow H–C_d–{}^\bullet C_d\ldots H–C_d–CH_2–C_d–H$	$k_{migration}$
(f) Sticking in 4 directions	$H–C_d–CH_2–C_d–H\ldots H–C_d–C_dH_2–C_d–H \rightarrow H–C_d–C_dH_2–C_d–H\ldots H–C_d–C_dH_2–C_d–H$	$k_{migration}$
(g) β scission	$H(g) + CH_3–CH_2–C_d–C_dH \rightarrow {}^\bullet C_d–C_dH + CH_3(g)$	k_β
(h) Surface radical migration	$HC_d–C_dH\ldots{}^\bullet C_d–C_dH \rightarrow HC_d–C_d{}^\bullet\ldots HC_d–C_dH$	…
(i) CH_x (x = 0-2) insertion into surface C–C bonds	$HC_d–C_dH + CH_x \rightarrow CH_{x+1}–C_d + {}^\bullet C_dH$	(x = 0), $k_{C-insert}$ (x = 1), $k_{CH-insert}$ (x = 2), $k_{CH_2-insert}$

process (c)) onto a more sound footing, this process is treated as a temperature-dependent activated process. Previous researchers have used quantum chemical methods to model the energy barrier for etching in a variety of microscopic models of the growing diamond surface.[16,29,30] The energy barriers were also used, together with transition-state theory, to obtain microscopic rate constants for etching. The barrier heights are, however, somewhat dependent on the level of quantum-mechanical theory used. This introduces an unknown uncertainty on the accuracy of rate constants determined in this way. While previous work has nevertheless led to good results, we have preferred here, as in our earlier studies, to use more empirical approaches to determining this important set of rate constants. Therefore, we used transition-state theory in the form of the Eyring equation to estimate the rate constant for CH_3 etching (k_{etch}, Table II, Eq. (9a)). The pre-exponential factor is given by $k_B T_s/h$, which is equal to $\sim 2.2 \times 10^{13}$ s^{-1} for a near-surface gas temperature of 1073 K. An accurate Gibbs energy of activation for this process has not yet been determined, although it is known from preliminary *ab initio* calculations[31] that $\Delta G^{\ddagger}_{etch}$ is in the range of 180-240 kJ mol^{-1}, considerably less than the C–C single-bond energy of ~348 kJ mol^{-1}. One goal of the KMC simulation is to determine an accurate value for $\Delta G^{\ddagger}_{etch}$ based on comparison of the calculated growth rates for different values of $\Delta G^{\ddagger}_{etch}$ with experiment.

C. Etch rate dependence on N_N (sidewall etching)

The 3D model also allows the etching to depend upon the environment, and in particular, upon the number of nearest neighbors, N_N, that are both bonded to the species being etched and on the same layer (see Figure 1). Two different approaches are adopted to model nearest neighbor effects upon etch rates. In the "linear model," the rate constant for etching is scaled by a factor $1/(aN_N + 1)$ in order to take some account of steric factors (Table II, Eq. (9b)). This is similar to the way Angus and Ponton modelled kink nucleation and propagation in diamond ⟨111⟩ step-edges.[32] The factor a is a parameter which can be altered to control the relative strength of the sidewall interaction.

Alternatively, the "exponential model" assumes that the extra bonding to the nearest neighbors can be allowed for by increasing the effective activation barrier for etching by a factor, ε, for every nearest neighbor (Table II, Eq. (9c)). ε is a variable which controls the effectiveness of sidewall bonding in inhibiting etching. The value of ε required to reproduce experimental observations can provide some insight into the etching process. For example, were etching to proceed via a mechanism in which all bonds are broken simultaneously in one reaction step, then ε would be expected to be large, close to one. This would yield a near-zero etching rate. However, etching from such sites could also involve a complex multi-step[16] mechanism, in which the sidewall species first undergoes an isomerization step—involving bond reorganization instead of merely bond-breaking—to yield a species that is less stable than the starting species, but possibly only by a small amount. Once such a species is formed, if it only has a single surface-carbon bond, then it can etch as in the normal etching process. The observed Gibbs energy of activation will reflect the value for standard etching, augmented by the Gibbs energy difference between the stable sidewall species and the rearranged form with a single surface-carbon bond. This can lead to a value of ε much

Reuse of AIP Publishing content is subject to the terms: https://publishing.aip.org/authors/rights-and-permissions. Downloaded to IP: 134.58.253.57 On: Tue, 19 Apr 2016 09:12:27

TABLE II. List of all rate equations and the parameters used in the model, most of which are obtained from Ref. 19, which should be consulted for definitions of all the symbols and units. Equations (9a)–(9c) are the modified versions of Eq. (9) to account for nearest neighbor interactions in the 3D model. Equations (12a)–(12c) are based on Arrhenius fits to the model for CH_x insertion in Refs. 20 and 24. For Eq. (12c), it is assumed that the inserting species is singlet CH_2 for which [$^1CH_2$] is ~1% of [CH_2].

$$k_{\text{activate}} = (k_1[\text{H}] + k_2)N_a \quad (1)$$

$$k_1 = 3.2\times10^{-12}\sqrt{T_{ns}}\exp(-3430/T_s) \quad (2)$$

$$k_2 = 1.66\times10^{-11}\exp(-49675/T_s) \quad (3)$$

$$k_{\text{deactivate}} = (k_3[\text{H}] + k_4[\text{H}_2])N_d \quad (4)$$

$$k_3 = 9.6\times10^{-13}\sqrt{T_{ns}} \quad (5)$$

$$k_4 = 3.2\times10^{-13}\sqrt{T_{ns}}\exp(-7850/T_s) \quad (6)$$

$$k_{CH_x\text{add}} = s_{CH_x} g_{CH_x}[CH_x]\bar{v}/4N_s \quad (7)$$

$$\bar{v} = \sqrt{8RT_s/\pi m_{CH_x}} \quad (8)$$

Etching/migration

$$\text{Original}: \quad k_{\text{etch}} = N_{\text{etch}}\times0.1k_{CH_x\text{add}} \quad (9)$$

$$\text{Eyring}: \quad k_{\text{etch}} = N_{\text{etch}}\frac{k_B T_s}{h}\exp\left(\frac{-\Delta G^{\ddagger}_{\text{etch}}}{RT_s}\right) \quad (9a)$$

$$\text{Linear}: \quad k_{\text{etch}} = \frac{N_{\text{etch}}}{(aN_N+1)}\frac{k_B T_s}{h}\exp\left(-\frac{\Delta G^{\ddagger}_{\text{etch}}}{RT_s}\right) \quad (9b)$$

$$\text{Exponential}: \quad k_{\text{etch}} = N_{\text{etch}}\frac{k_B T_s}{h}\exp\left(-\frac{\Delta G^{\ddagger}_{\text{etch}} + N_N\varepsilon\Delta G^{\ddagger}_{\text{etch}}}{RT_s}\right) \quad (9c)$$

$$k_{\text{migration}} = N_{\text{mig}}A_{\text{mig}}\exp(-E_{a,\text{mig}}/RT_s) \quad (10)$$

$$k_\beta = N_\beta\frac{k_B T_s}{h}\exp(-1.8\times10^5/RT_s) \quad (11)$$

Insertions

$$k_{C-\text{insert}} = 8.587\times10^{-11}\times\exp(-19\,836/RT_s) \quad (12a)$$

$$k_{CH-\text{insert}} = \exp\{2\times10^6\times(1/T_s)^2 - (18\,700/T_s) - 24.92\} \quad (12b)$$

$$k_{CH_2-\text{insert}} = k_{CH-\text{insert}}\times0.1 \quad (12c)$$

smaller than 1. Determining a value for ε that yields acceptable agreement with observed behavior is another goal of the KMC simulation.

To determine which model for sidewall etching is a more accurate description of the real process, the simulation was performed with zero CH_4 input and all growth processes turned off, and only etching by H/H_2 allowed. No defects (see Sec. II E below) were included. The evolving surface morphology was viewed continuously during the simulated

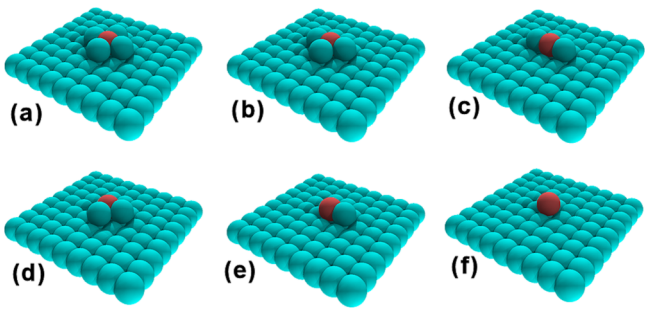

FIG. 1. The different geometric configurations for a species to be etched (red) which have different etching rates, with N_N values of (a) 4, (b) 3, (c) and (d) 2, (e) 1, and (f) 0.

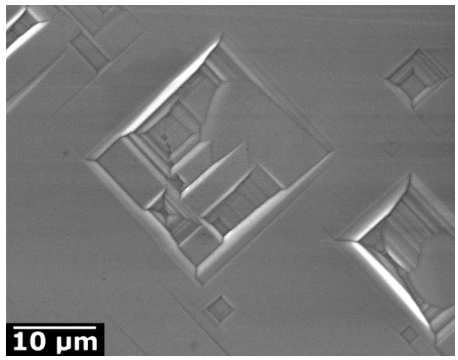

FIG. 2. Rectangular etch pits formed on the (100) surface of a single-crystal diamond following etching in H_2 in a microwave plasma CVD reactor.[24]

etch process, with the aim being to find values for the parameters a or ε that reproduced the rectangular etch pits seen in experiment, such as those shown in Figure 2.

D. Critical nucleus

It has been speculated that one important difference between 2D and 3D simulations may be the nature of the "critical nucleus." As hydrocarbon species adsorb onto the surface or migrate around, they may meet and stick to an existing adsorbed species and bond to them forming an "island." If more species are added to it, this island may be the beginning of a new layer of growth. However, carbons can also be etched away from the side of the island, maybe eventually etching it away completely. The critical nucleus is the smallest cluster of sp^3-bonded carbon that remains on the surface eventually to become a new layer of diamond.

In two dimensions, the critical nucleus was simply 2 adjacent carbon atoms on the surface. When two such atoms meet, either by a gas-phase methyl adsorbing directly next to an already-adsorbed CH_2 group (ER growth) or by two migrating CH_2 groups meeting on the surface (LH growth), they may bond together and become immobile. Unless one of them is subsequently etched away, this immobile pair (the critical nucleus) provides two new sidewalls onto which later carbons can attach.

However, in three dimensions, the size of the critical nucleus is less obvious because adsorbed $CH_2^\bullet$ species bonded laterally to sidewalls etch away at a slower rate than isolated $CH_2^\bullet$ groups (via the parameters a and ε, mentioned above). Therefore, the size and the shape of the critical nucleus will reflect a competition between the rate at which species add to an island (by the ER or the LH routes) compared to the rate at which species at the edge/corners of the island are etched away. It has been suggested that on a real 3D growing surface, the critical nucleus may comprise as many as four carbons,[33] possibly arranged in a square, as this provides a stable structure with each carbon having $N_N = 2$ making them all difficult to etch.

In order to characterize and identify the critical nucleus, we require a quantity from our simulation which describes the formation of a new layer from a critical nucleus. We chose to count the number of creation and annihilation events which occurred for a range of different sized and shaped surface

Reuse of AIP Publishing content is subject to the terms: https://publishing.aip.org/authors/rights-and-permissions. Downloaded to IP: 134.58.253.57 On: Tue, 19 Apr 2016 09:12:27

islands during growth simulation. We counted "monomer creations" when a single species landed on the surface and bonded into the lattice, and "monomer etching" when a single adspecies with no neighbors desorbed. In practice, monomer creation events are rare, because in our model, isolated adspecies only form temporary attachments to the surface, instead migrating around until they meet an existing island or are etched away. Such transient single-species' addition and creation events were not counted because no permanent change to the diamond surface had occurred. The rare exceptions to this occurred when adsorbing defect species were deliberately included (see Sec. II E), or when sidewall etching of a surface 2×1 group led to the creation of an isolated but permanently bonded adatom.

"Dimer creation" occurs when another species bonds to a transient or permanently bonded monomer (via LH or ER routes), and "dimer etching" when an atom etches away from a dimer. Similarly, "trimer creation" is when a species adds to an existing dimer either linearly or in an "L"-shape, and "trimer etching" when one of the 3 species etches away. "Quadramer creation" and "quadramer etching" follow a similar approach, except that now the various quadramer geometries needed to be taken into account including 2×2, 1×4 linear, and "L," "T," and "S" shaped structures. Structures containing 5 or more adatoms are considered together as large islands.

Comparing the number of creation events to annihilation events for each size of surface island allowed the program to distinguish between islands which are transient (i.e., those which etched faster than they grew) and those which ultimately led to layer formation. The smallest island which grew faster than it etched was considered to be equivalent to the critical nucleus. This comparison was performed over the time interval of the whole simulation, as well as for time intervals consistent with the growth of a monolayer at the beginning of the simulation (i.e., when the surface as initially flat), approximately halfway through, and at the end of the simulation. This was a check to ensure that the critical nucleus obtained by this method was not a function of initial conditions.

E. Non-etchable defects

From experimental measurements, we know that etching pristine flat diamond surfaces in hydrogen are extremely slow due to the low probability of etching an atom fully embedded in a terrace ($N_N = 4$). However, most natural and lab-grown diamonds contain defects, especially threading dislocations which run perpendicular to the growth surface and which provide points of weakness on the surface with a higher etch rate than the surrounding atoms. The exact nature of this defect at the surface, whether it is an atom which is not fully embedded ($N_N < 4$), or bonded via strained bonds (ε smaller than normal), or a crooked geometry, is not clear. Nevertheless, it can be modelled by simply assigning an etch-parameter, b, to the defect site, which defines how much easier it is to etch this particular defect atom than a normal surface atom. Thus, $b = 1000$ means that the defect atom has an etch rate 1000× greater than the surrounding atoms (with the same N_N). To simulate a threading dislocation, when the defect atom is etched, the atom immediately beneath it inherits its predecessor's enhanced etch rate. Thus, as each defect atom etches, the defect propagates downwards.

In order to simulate random non-epitaxial growth and defect formation, such as twins and dislocations, routines were added to the KMC code that allowed unetchable, immobile $1 \times 1 \times 1$ blocks to be added to the initial surface in predefined or random locations or to be added randomly during the growth process with a chosen rate relative to that for CH_3 adsorption. For etching, these "defect" blocks represent easily etchable weak points on the surface, whereas for growth, they represent species such as N or CN which are believed to adsorb onto the surface when N_2 is added to the CVD gas mixture and act as special 1-atom critical nuclei. In cases where the rate-limiting step for diamond growth is the time required to create the first critical nucleus on a new layer, only a very small number of these defects may be required to increase the growth rate greatly, the minimum being only 1 defect site per layer. Such defects would effectively "catalyse" diamond growth and may even change the crystallite morphology, while becoming incorporated into the diamond in only trace amounts.[33]

Other adjustable parameters, b and g, are used to control the etch rate and growth rate, respectively, on these rare defect sites relative to those on the majority non-defect sites. For $b > 1$, the defect etches faster than the surrounding lattice and etching produces a hole in the surface exposing a new surface site from the underlying layer. There are now two possibilities for the newly exposed surface site: either the new site is the same as the other surface sites and is treated accordingly, or it may be another defect site. For the latter case, a defect site propagating downwards following etching simulates having a pre-existing dislocation in the substrate. Such dislocations are known to thread for distances of the order of 10^2 μm perpendicular to the growth direction, even in near-perfect single-crystal diamond films and high-pressure high-temperature (HPHT) substrates used as seed crystals for epitaxial growth.[34] In the model, if defects are permitted to propagate downwards, then with $b > 1$, the newly revealed defect site at the bottom of the hole also etches faster than its surroundings. Thus, the relative etch rate parameter, b, controls whether the surface etches back uniformly or whether an etch pit forms together with its size and shape.

In a similar fashion, growth rates on a defect site may be enhanced ($g > 1$) or inhibited ($g < 1$) relative to those on the standard diamond surface. For net growth and with $g > 1$, and with the condition set so that blocks that adsorb onto the defect site inherit the defect's value of g, the new block turns into a new surface defect site. Thus, the defect propagates upwards at a rate governed by the value of g, simulating growth of a grain boundary, dislocation, hillock, or twin plane. Alternatively, if $g < 1$ or defects are not allowed to propagate upwards, then the defect can simply be overgrown by the rest of the lattice creating an isolated, buried defect.

III. RESULTS

The base set of conditions used in these simulations was those for deposition of standard MCD in a hot filament reactor, given in Ref. 20, Table I. The first task was to determine

Reuse of AIP Publishing content is subject to the terms: https://publishing.aip.org/authors/rights-and-permissions. Downloaded to IP: 134.58.253.57 On: Tue, 19 Apr 2016 09:12:27

the minimum grid size and the simulation time (or number of layers grown) for which the simulation was statistically equilibrated, i.e., that the value for the required output parameters had reached a steady-state average with little noise, while minimising computation time. By monitoring the growth rate and surface roughness as a function of simulation time, we determined that a 25×25 grid along with 10 layers growth were the minimum values required to obtain consistent output.

Critical parameters in the model were then systematically varied in order to test the sensitivity of the model and results to some of the input parameters and other variables that are not known accurately. It was found that the growth rates and surface roughness are most sensitive to the concentration of CH_3 and to the desorption rate constant, because the interplay between these parameters directly affects the rate of adsorption. Variations of ~10% in the other gas concentrations [H] and [H_2], or to the gas/substrate temperatures, or the other rate constants, did not affect the output as significantly.

A. Etching

The first task was to determine a reliable value for the rate constant for etching isolated adspecies, k_{etch}, by varying the value for $\Delta G^{\ddagger}_{etch}$ in Eq. (9a) and comparing the calculated net etch rate with that from experiment. Simulations were run on a 50×50 grid for 50 s of KMC time under the standard MCD conditions used previously. Simulations were run using the new expression for the rate constant, using different values of $\Delta G^{\ddagger}_{etch}$ between 0 and 350 kJ mol^{-1}. Results were obtained by averaging over 21 runs for each value. The results (Figure 3) show that the growth is very sensitive to the etching rate, more so than to any other parameter in the model. When $\Delta G^{\ddagger}_{etch}$ is small, k_{etch} is very large and etching dominates so there is virtually no net growth. Conversely, when $\Delta G^{\ddagger}_{etch}$ is large, there is no etching and the growth rate is a maximum, limited only by the flux of species to the surface. The maximum growth rate that the model produces under MCD conditions when there is no etching is ~0.85 μm h^{-1}, larger than the experimental value by a factor of two. Because of the exponential dependence of etching rate upon $\Delta G^{\ddagger}_{etch}$, there is only a small range of $\Delta G^{\ddagger}_{etch}$ values for which significant growth is possible in the presence of etching. Thus, further calculations were performed in this range showing a roughly linear increase in growth rate between the no-growth and no-etching limits. Interpolation allowed a value within this range of $\Delta G^{\ddagger}_{etch}$ = 200 kJ mol^{-1} to be chosen that produced a calculated etch rate that agreed with the experimental rate, and this was used for all subsequent calculations. We note that this value is similar to that used in our previous 2D simulations (186 kJ mol^{-1}[29]) and consistent with the value suggested by the recent preliminary *ab initio* calculations.[31]

B. Sidewall etching

Recall that in the "linear" etching model, the effect of the N_N neighboring C–C bonds on the etch rate is treated approximately by simply assuming that they lead to a linear decrease in the rate of etching. Thus, the rate for etching a sidewall species is given in Eq. (9b). This model produces a relatively weak dependence of etch rate upon N_N. For example, for $a = 1$, an adspecies that is entirely surrounded by adjacent atoms ($N_N = 4$, Fig. 1(a)) and can only by attacked from above will have an etch rate only 5 times lower than that for an isolated adspecies (Fig. 1(f)). In this case, we found that etching occurred randomly across the surface, leading to a spikey morphology sometimes referred to as "grass" (see Figure 4(a)). Increasing the value of a simulates the case where sidewall bonds have a greater effect upon etching probability than the bond to the surface. Nevertheless, random etching and the grass morphology remained prevalent even when the value of a was set to unrealistically high values such as 100. The reason for this can be discerned from Eq. (9b). Although there is a potentially huge decrease in etch rate of $1/(a + 1)$ when going from zero to one neighbor, the decrease in etch rate for additional neighbors is much lower, typically only an additional factor of ~2 for each extra neighbor beyond 1. Thus, isolated atoms ($N_N = 0$) etch immediately, but atoms with 1-4 neighbors etch more slowly but with all configurations etching at roughly the same rate, leading to random grass. Clearly, the

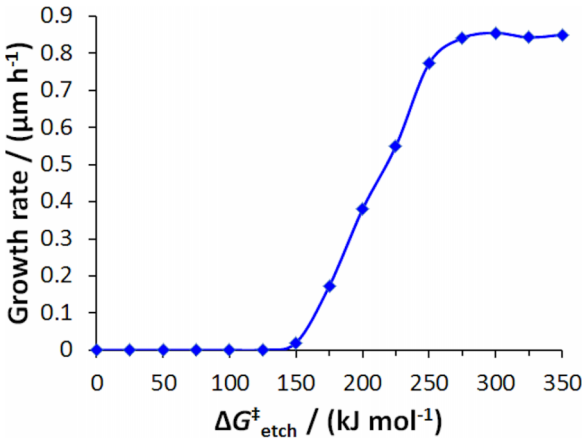

FIG. 3. The variation of the calculated diamond growth rate under MCD conditions as a function of the Gibbs energy of activation for etching, $\Delta G^{\ddagger}_{etch}$ (see Table II, Eq. (9)).

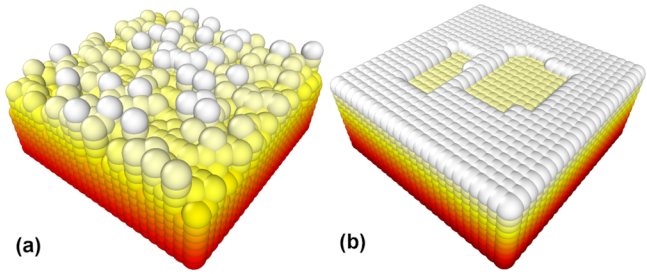

FIG. 4. Simulation of etching the 100 diamond surface, with no defects included. The surface was initially flat with dimensions $25 \times 25 \times 10$ and has been color-shaded in the z-direction to allow different layers to be distinguished. (a) Etching using the linear model with $\varepsilon = 0.1$. Etching surface atoms occurs at random locations leading to a "grass" like topography. (b) Etching using the exponential model with $\varepsilon = 0.365$. The initial etch rate is extremely low, until one atom is etched, and then the surface rapidly etches laterally to form rectangular etch pits. The areal density of the etch pits depends on the value of ε. Eventually, the entire layer is removed, often before the underlying layer has started to etch. This leads to slow, layer-by-layer etching.

Reuse of AIP Publishing content is subject to the terms: https://publishing.aip.org/authors/rights-and-permissions. Downloaded to IP: 134.58.253.57 On: Tue, 19 Apr 2016 09:12:27

linear model does not reproduce the smooth etching, with or without etch pits, seen in experiment, and so can be discounted as a viable model.

In the "exponential" etching model, one has a more microscopically physically justifiable model for the effect of neighbors on the etch rate. A series of reorganization steps, each with Gibbs energy cost of $\varepsilon \times \Delta G^{\ddagger}_{\text{etch}}$, is assumed to be needed to go from the starting species to a hypothetical pre-etching species with only a single bond to the surface. The latter then etches with the same $\Delta G^{\ddagger}_{\text{etch}}$ as an isolated adatom. For N_N neighbors, N_N such reorganization steps are assumed to be needed. This leads to an overall apparent activation free energy of $\Delta G^{\ddagger}_{\text{etch}} + (N_N \times \varepsilon \times \Delta G^{\ddagger}_{\text{etch}})$, where ε is the ratio of the Gibbs energy cost for breaking a lateral C–C bond to the Gibbs energy of activation needed to break the vertical bond to the surface ($\Delta G^{\ddagger}_{\text{etch}}$), as in Eq. (9c). In this case, for a species with $N_N = 1$ and with ε set to a value of 0.1 (as mentioned previously), the etch rate will be ~10% of that of an isolated adspecies, while for $N_N = 2$, the relative rate drops to 1%, and so on. Despite this, simulations showed that using values for $\varepsilon = 0.1$ produced random etching and grass morphology, similar to that shown in Fig. 4(a).

Increasing ε values produces an even stronger dependence of etch rate upon N_N. For example, with $\varepsilon = 0.365$, the etch rate decreases by a factor of ~3000 for every neighbor (i.e., etch rate scales as (3000^{-N_N}), so that for a species with $N_N = 4$, the etch rate is $\sim 10^{-14}$ times that of an isolated adspecies, making it extremely difficult to remove atoms fully embedded in a flat terrace, consistent with the very low etch rates observed experimentally. This value for ε simulates the observed etch morphologies well, as shown in Fig. 4(b). For a pristine, flat surface, the initial etch rate is very low because all the atoms have $N_N = 4$, and so, no etching happens for a long time. But eventually, an atom is etched from the surface leaving a hole, which exposes four sidewalls. These sidewall atoms (each with $N_N = 3$) have a much higher probability (3000×) of being etched than any of the other surface atoms which all still have $N_N = 4$, so they are removed first, enlarging the hole outwards and exposing further sidewalls. As a result, the hole rapidly etches laterally and opens up to form a square etch pit. The etch pit increases in size until the whole layer has etched away, exposing the lower pristine layer, and then the cycle begins again. Because of the symmetry of the grid, the etch pits are square, although the random nature of the etching allows the shape of the pit to vary continuously during the process from square to rectangular. The value of $\varepsilon = 0.365$ was used in all subsequent calculations, and we shall return to the simulation of etch pits in Sec. III D.

C. Critical nucleus

An analysis of the critical nucleus was done for all 4 growth regimes for up to 10 layers of growth, and the results are shown in Fig. 5 for the two extremes, SCD and UNCD growths. For all 4 growth regimes, it was found that island growth occurred for all sizes of island except size 1. As explained in Sec. III D, permanently bonded monomers are quite rare on the surface, and if formed, they mostly etch away before another species can adsorb or migrate next to them to

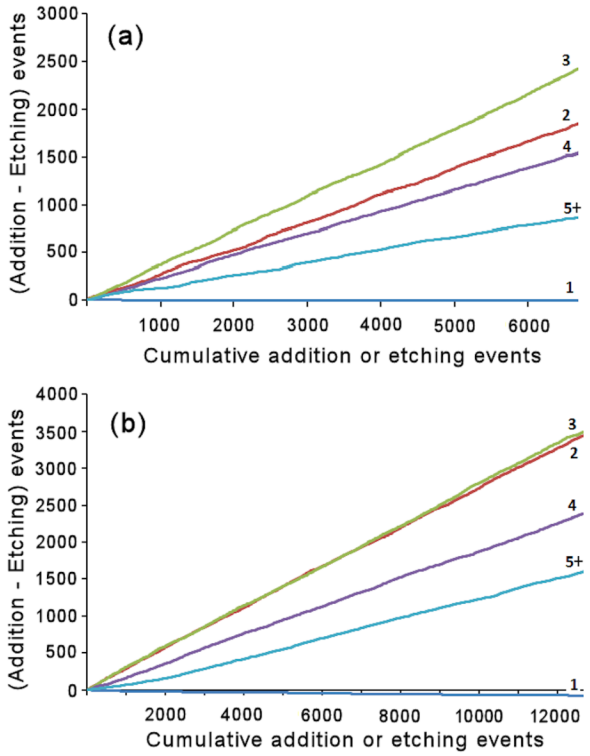

FIG. 5. The difference between creation events and etching events following simulated growth of 7 layers of diamond on a 50×50 grid for (a) SCD and (b) UNCD conditions. The plots show the effective island growth rate for islands of sizes 1, 2, 3, 4, and 5 or more. A positive slope indicates islands grow faster than they etch away, i.e., the island size increases leading to net growth of a diamond layer. In contrast, a negative slope, which only occurs for island sizes of 1, means that they etch away faster than they grow, and so, these islands are transient.

form a larger island. Thus, the smallest island that leads to growth is size 2, so we can conclude that a 2-carbon dimer constitutes the critical nucleus for all types of diamond growth in 3D. This is not surprising given that etching of atoms that have bonded to a sidewall is so unfavorable (see Sec. III D below); once they have permanently attached themselves to an island, very few sidewall atoms are ever etched away. Thus, the shape and geometry of islands are not modified by sidewall etching, and so two bonded surface atoms are all that is required to initiate the new layer.

Comparing Fig. 5(a) for SCD and Fig. 5(b) for UNCD conditions, we can see that the net island growth rate for trimer islands exceeds that for dimers in the case of SCD, but is equal to it for UNCD. It is statistically far more likely to have more small islands than larger ones, so we would expect the island growth rate to decrease in the order 2, 3, 4, 5+ (with 1 having a "negative" growth rate due to etching, as mentioned above). However, this ordering needs to be modified based on the rate at which species stick to the sidewall (which, in turn, is related to the size of the island, i.e., the length of the perimeter sidewall). For dimer creation to occur, a monomer must stick to another monomer, which on a cubic grid can be attacked from any of 4 directions. For a trimer creation, a monomer must stick to a dimer, which can be attacked from 6 directions, and for quadramer creation, the trimer islands can be attacked from 8 directions. Thus, just

Reuse of AIP Publishing content is subject to the terms: https://publishing.aip.org/authors/rights-and-permissions. Downloaded to IP: 134.58.253.57 On: Tue, 19 Apr 2016 09:12:27

on probability grounds, the rate of trimer creation should be 50% faster than that for dimer creation, while the rate for quadramer creation should be double than that for dimers. The competition between the decreasing rate due to island size prevalence and the increasing rate due to probability of attack leads to a maximum in the rate, which occurs between island sizes of 2 and 3. The maximum shifts more towards 3 for conditions where there is more opportunity to sample the sidewalls, i.e., when there is the greatest surface migration as in SCD growth. When there is little or no surface migration, as in UNCD, the maximum shifts towards 2. Repeating these comparisons with different time intervals or with time intervals consistent with a monolayer growth at the start, middle, and end of a 20-monolayer simulation run gave the same results. This showed that the conclusions about critical nucleus size and behavior are not governed by the initial starting conditions.

D. Defects and etch pit simulations

We now return to the subject of etch pits discussed earlier in Secs. II E and III B. The simulation was initialized with a single defect atom located in the center of the grid, and b varied from 0 to 50000. For $b > 20000$, the defect etch rate was too fast, and etching simply produced a 1-atom-wide hole vertically through the sample. But for lower values of b, there is a balance between the lateral etch rate for the etch pit widening and the defect etch rate which would reveal the underlying layers. Fig. 6(a) shows the etch pit formed with $b = 10000$, which is an inverted square-based pyramid with a sharp point at its base. This is very similar to the shape and size of etch pits seen experimentally when etching diamond with O_2 mixtures.[13] Reducing b to 1000, as in Fig. 6(b), lowers the relative defect etch rate and produces shallower rectangular etch pits with flat bottoms, which more closely resemble those seen when etching diamond in H_2,[12] as seen previously in Fig. 3.

When CH_4 is introduced into the gas mixture, these etching processes now compete against adsorption, migration, and growth. Single defect sites may play a role under net growth conditions as well, since they can act as a preferential nucleation site for adsorbing and migrating carbon groups. In other words, the sticking coefficient at a defect site may be larger than that for a flat terrace site, and this may be quantified in the model by a factor g, which sets the relative growth rate on this site compared to non-defect sites. With $g < 1$, direct growth on the defect site is disfavored, but this makes little difference to the overall film growth as any holes in the terrace that result from this are quickly filled by migrating C atoms which fall in and become trapped. Conversely, for $g > 1$, growth on the defect site is now favored, but for a single isolated defect, again, this has little effect upon the overall growth. However, if we allow the defect to propagate upwards (as described in Sec. II E), modelling the effect of a lattice mismatch, grain boundary, or dislocation being replicated as the film grows, then changing the magnitude of g produces different effects. For very large g, such as 1000, we obtain needle-like growth (see Fig. 7(a)) which is rather unrealistic in terms of CVD diamond growth (but which has been seen in other CVD systems), whereas for smaller values of $g \sim 10$-100, we see the formation of more rounded "hillocks" (Fig. 7(b)) which are very similar in size, shape, and morphology to those often seen when growing diamond on defective SCD substrates.[35]

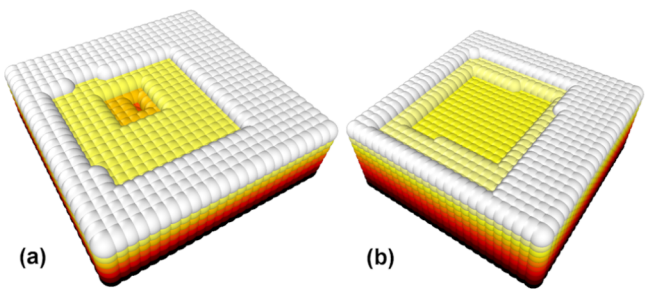

FIG. 6. Simulated etch pits in the (100) diamond surface created with all growth processes turned off (i.e., no C species striking the surface). The surface initially had a single defect site which was allowed to propagate downwards when etched using the values $\varepsilon = 0.365$ and (a) $b = 10000$ producing an inverted pyramid with depth:width ratio ~5/16, and (b) $b = 1000$ producing flat-bottomed pits with depth:width ratio ~1:7.

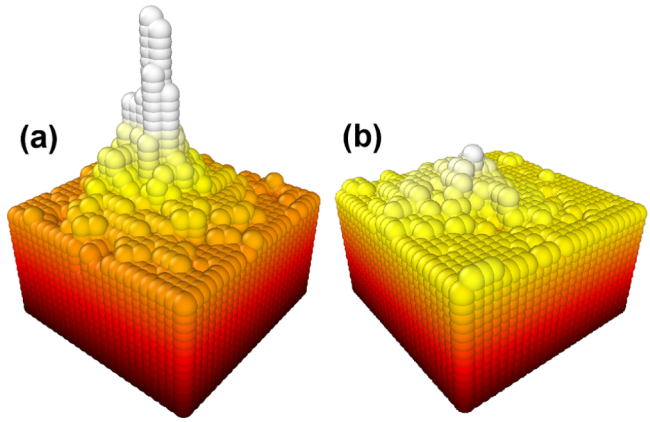

FIG. 7. Simulated growth features created on the (100) diamond surface. The surface initially had a single defect site which was allowed to propagate upwards. Using the values $\varepsilon = 0.365$ with (a) $g = 1000$ creates a sharp needle-like feature, and with (b) $g = 100$ creates a more realistic-looking hillock structure.

E. Multiple defects

To simulate the effect of defects being formed continuously during the growth process by random adsorption of species such as N or CN, or C, CH, CH_2 (see Sec. III F), the program includes a routine which can convert an adsorbing CH_x species to an immobile, unetchable defect block with a user-defined probability. The probability, P_{def}, of such defect adsorption was varied from 1.0 (every species that lands on the surface becomes a defect) to 10^{-4} (only one in 10000 adsorbing species becomes defects) and the effects upon the diamond growth rate and film roughness under MCD growth conditions are shown in Fig. 8. Note that for the 50×50 block grid used in these calculations, there are 2500 blocks in a monolayer, so for defect probabilities more than 1/2500 ($P_{def} > 4 \times 10^{-4}$), on an average, there will be more than one defect per layer.

Reuse of AIP Publishing content is subject to the terms: https://publishing.aip.org/authors/rights-and-permissions. Downloaded to IP: 134.58.253.57 On: Tue, 19 Apr 2016 09:12:27

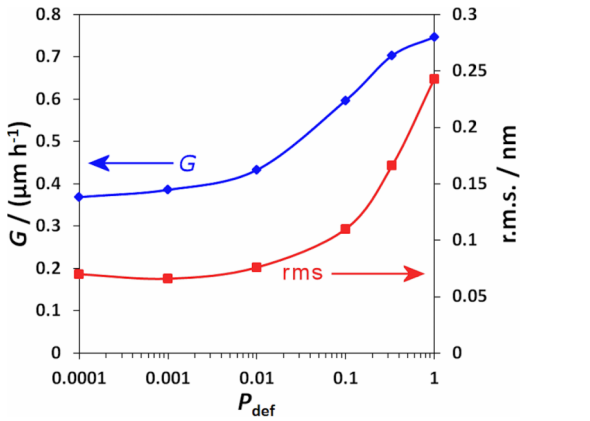

FIG. 8. Growth rate, G, and r.m.s. surface roughness as a function of P_{def}, the probability of an adsorbing CH_x species forming an unetchable, immobile surface defect, calculated for MCD growth conditions on a 50×50 block grid, and with $b = 0$, $g = 1.0$, and $\varepsilon = 0.365$, and defects not propagating upwards.

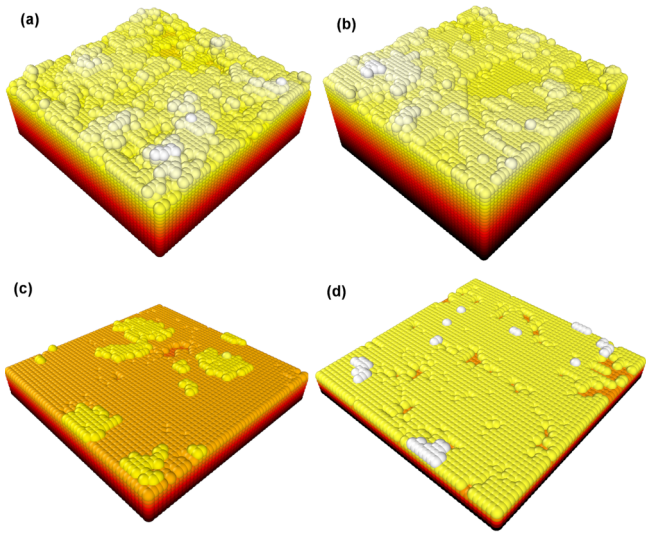

FIG. 9. 3D projections of the surfaces generated by the 3D model representing diamond growth under different process conditions. (a) UNCD, (b) NCD, (c) MCD, and (d) SCD. The layers have been colored to make it easy to distinguish individual layers.

Fig. 8 shows that with increasing numbers of defects, the growth rate increases and the surface becomes rougher. Surprisingly, the defect probability needs to reach an unexpectedly high value ≥0.01 before the changes in the growth rate or roughness become significant. Experimental observations, on the other hand, report that small concentrations of ppm, say N_2, in the gas phase can increase growth rates by similar factors, and tiny variations in N_2 concentrations in the gas feed or vacuum integrity can make day-to-day process control very tricky.

To determine the likely values for P_{def} in N-containing gas mixtures used for diamond growth, the concentration profile for a 1.5 kW microwave plasma reactor operating at 150 Torr and substrate temperature of 1110 K with a gas mixture of 4.4% CH_4/0.6% N_2/H_2 was calculated[36] using the gas-phase model described in Ref. 20. These concentrations were then extrapolated back to a height of 50 μm above the growing diamond surface using the procedure in Ref. 28, giving values of 1.8×10^{10}, 2.12×10^{9}, 2.70×10^{9}, and 5.25×10^{6} cm^{-3}, for N, NH, NH_2, and CN, respectively. Thus, by far, the most abundant N-containing reactive species at the diamond surface is atomic N. With $[CH_3] = 6.6 \times 10^{13}$ cm^{-3}, this makes the ratio $[NH_x$ (x = 0-2)]:$[CH_3]$ = 1:~3000. If these NH_x species are presumed to be solely responsible for surface defects, then their corresponding P_{def} value is $\sim 3 \times 10^{-4}$, which is 30 times smaller than the values in Fig. 8 that begin to affect growth rate and surface roughness. Thus, the model[33] for defect formation and growth enhancement, in which N, CN, or NH_x species form immobile, unetchable surface defects which catalyse growth, may be incorrect or at least not the complete story.

F. Simulations using different growth conditions

Figure 9 shows simulated surface morphologies after growing for several layers under UNCD, NCD, MCD, and SCD conditions, while Table III gives some of the relevant growth details. The 3D model can predict growth rates that are within a factor of two for all the 4 types of diamond growth considered, although some of this agreement may be due to the empirical choice of $\Delta G^{\ddagger}_{etch}$.

By watching the simulation as it builds up the diamond layers, we can see that under SCD and MCD conditions, growth proceeds via migration and step-edge attachment (see Fig. 9). For SCD, this leads to predominantly large, flat terraces with little variation in surface height (Fig. 9(d)). Here, diamond growth proceeds by the formation of a critical nucleus which then increases in size as nearby adsorbed species migrate to it and adhere to its sidewalls. This is due to the long average surface-diffusion length, ℓ (defined as the mean distance measured in a straight line from its initial adsorption site that a migrating species has travelled when its migration is permanently terminated by processes such as etching and attachment to the lattice) of 5 which enables the adsorbed species to migrate for long enough that it can find a step-edge upon which to attach. The high H atom concentration aids this migration process by increasing the rate of creation and termination of surface defects which is often the rate-limiting step for surface CH_2 migration. The island sizes grow as large as 100-200 species before a second layer nucleates on top. Thus, it appears that for SCD, islands grow and coalesce on a single layer before subsequent layers begin.

For MCD, the situation is very similar, except that the average size of the islands before the subsequent layers begin is reduced (Fig. 9(b)). For NCD growth, the growth process starts to change, as now the rate of forming new nuclei and initiating new islands, which may be on an upper layer, equals or exceeds the rate at which migrating species adhere to step edges (Fig. 9(c)). This arises because the surface migration rate is lower, leading to a smaller average surface-diffusion length of l–2. This results in a large number of small (<5 species) islands, and growth switches from mainly LH to mainly ER processes. Finally, for UNCD (Fig. 9(a)), the migration rate is so low compared to the adsorption rate that ER kinetics dominate, resulting in a nearly randomly arranged surface with little or no island terraces visible.

Reuse of AIP Publishing content is subject to the terms: https://publishing.aip.org/authors/rights-and-permissions. Downloaded to IP: 134.58.253.57 On: Tue, 19 Apr 2016 09:12:27

TABLE III. Diamond growth rate, G, and r.m.s. surface roughness, R, for 4 growth regimes calculated using the exponential model for sidewall etching, and using $\Delta G^{\ddagger}_{etch} = 200$ kJ mol^{-1}, $\varepsilon = 0.365$, and with no defects included. Also shown is the mean surface migration distance, ℓ, and the fraction of surface monoradical sites, F_{mr}, plus the percentage of the growth that results from ER direct adsorption processes and from LH migration processes. The values for the number of other process that occur are quoted relative to that for the number of CH_3 species that adsorbed. These processes include the total number of adspecies etched (excluding β scission), the number of adspecies etched by β-scission reactions, plus the number of adsorption processes for the three CH_x species. The relative number of insertion processes was 0.0 for CH_2 and CH species for all deposition conditions, but that for atomic C insertion was significant and has been included in the table.

	G/ (μm h^{-1})	R/nm	ℓ/atoms	F_{mr}	%ER	%LH
SCD	0.533	0.057	5.2	0.089	58	42
MCD	0.39	0.077	1.5	0.118	84	16
NCD	2.3	0.086	0.95	0.113	86	14
UNCD	0.068	0.12	0.56	0.048	93	7

Number of events relative to the number of CH_3 adsorptions

				Adsorption		
	Etching	β−scission	C insertion	CH_2	CH	C
SCD	0.050	1.4×10^{-4}	0.040	1.6×10^{-3}	1.6×10^{-4}	4.2×10^{-3}
MCD	0.57	2.5×10^{-4}	0.012	7.0×10^{-5}	4.1×10^{-5}	1.2×10^{-3}
NCD	0.34	4.8×10^{-4}	0.0018	6.7×10^{-5}	0.0	1.6×10^{-4}
UNCD	0.65	1.9×10^{-4}	0.0	5.4×10^{-6}	0.0	0.0

Table III also shows that the simulation correctly predicts the increasing roughness in going from SCD to UNCD. It also quantifies the change in growth process from predominantly ER processes (adsorption and random attachment) for UNCD to an almost 50% contribution from LH processes (adsorption, migration, and step-edge attachment) in SCD growth. One of the striking differences between SCD growth and the other 3 types of diamond is in the greatly reduced relative number of adsorbed species that are etched off the surface. For the 3 other diamond types, typically 34%-65% of adsorbed carbon species are etched back into the gas phase before they can permanently bond into the lattice. But for SCD, this number is reduced to ~5%, meaning that 95% of all carbons that adsorb ultimately become part of the diamond lattice. Again, this can be explained by the increased probability of incorporation of a species the more opportunity it has to sample different surface neighborhoods.

Table III also shows the number of adsorptions that arise from C, CH, and CH_2 relative to those from CH_3, the species primarily responsible for diamond growth. For SCD and MCD, these other species contribute about 1% of the carbons in the final lattice. Although small, this is significant enough for these species (especially atomic C) to be considered as candidates for defect-forming species, such as those modelled in Sec. III E above. In contrast, for NCD and UNCD growths, these species contribute <0.1% of the carbons in the final diamond lattice, and so probably cannot be responsible for the extensive renucleation processes that occur in these cases. Instead, they may be responsible for the rarer type of growth defect that only becomes apparent during layer-by-layer growth, and thus eliminating these might be one way to improve the quality of SCD.

Finally, Table III shows that inclusion of C-insertion reactions into the growth model is only necessary for SCD and MCD conditions, where they contribute ~5% and 1% of the carbons in the lattice. These values are sufficiently large that C-insertions can also be considered candidates for defect-forming processes. Once inserted, incorrect restructuring of the adspecies may create a misaligned defect species leading to renucleation and/or twinning. Detailed molecular modelling of suitable processes is suggested as a follow-on to this work.

IV. CONCLUSIONS

We have investigated the parameter space of our 3D KMC model of CVD diamond growth. By performing a large number of simulations covering a wide range of deposition conditions, we have been able to show how trends in changes to our kinetic model reflect the underlying chemical kinetics of the CVD system. Our study shows that a more accurate description of the fundamental chemical processes, in particular, the temperature dependence of etch rates and surface deactivation processes, leads to a more accurate prediction of macroscopic growth properties. The model predicts growth rates that are dependent upon temperature, and which are consistent with those from experiment. It suggests that growth of good quality facetted diamond occurs via a Langmuir-Hinshelwood process in which adsorbed carbon species migrate across the surface to adhere to step-edges forming islands. The size of these islands varies depending upon growth conditions and can contain tens or hundreds of carbon species for SCD and MCD, but as little as 5 for NCD. UNCD growth is dominated by Eley–Rideal kinetics in which the carbon species bond wherever they happen to land with little or no surface migration.

When etching is modelled as a temperature-dependent activated process, the KMC model is extremely sensitive to the value of the Gibbs energy of activation, $\Delta G^{\ddagger}_{etch}$, which is a parameter that unfortunately is difficult to measure experimentally. However, a value of 200 kJ mol^{-1} for $\Delta G^{\ddagger}_{etch}$

Reuse of AIP Publishing content is subject to the terms: https://publishing.aip.org/authors/rights-and-permissions. Downloaded to IP: 134.58.253.57 On: Tue, 19 Apr 2016 09:12:27

reproduces the experimental growth rates quite accurately, and so, this can be taken as a reasonable first approximation.

The sidewall etch parameter required to match the experimental shape of the rectangular etch pits was $\varepsilon \sim 0.365$ in the exponential model, which equated to each lateral neighbor making a target atom ~3000 times harder to etch. In the exponential model, the value of 0.365 makes sense chemically, as it implies that the Gibbs energy cost associated with rearranging the bonding at a sidewall to form singly bonded carbon species is much less than the Gibbs energy cost of fully breaking a bond, but is still large enough to make etching of such sites harder than for an isolated adatom.

Various models for defects were studied. Allowing a selected block to etch faster than other blocks simulated a defect site in the lattice that acts as a "weak point" on the surface, such as a dislocation. Choice of a suitable value for the relative etch rate parameter, *b*, allowed etch pits to be simulated with size, shape, and geometry consistent with those seen experimentally. In contrast, by allowing carbons on defective sites to be more reactive than normal surface carbons, growth preferentially occurs on the defect sites, propagating the defect upwards, just as is seen when growing CVD diamond onto seed crystals with surface dislocations. Values of the "stickiness" parameter *g* of 10-100 produced hillock structures similar to those seen in experiment.

Allowing defect blocks to adsorb with random probability tested the model for growth-rate enhancement by the catalytic effect of surface adsorbed defects, such as N and CN. These are assumed to form unetchable, immobile defects which act as critical nuclei for new layer formation. Although an effect consistent with this was found using the simulation, the concentration of surface defects (1 in every 100 carbons) needed to noticeably increase the growth rate or roughen the surface was 30 times higher than the expected concentration of likely defect species in these growth conditions. Therefore, the results suggest that the model for catalytic enhancement by surface defects is not the complete answer to this problem.

By watching the layers grow during the simulation, two features of the growth process became apparent. First, as the quality of the diamond film worsened, i.e., on going from SCD to UNCD, the number of growth islands present at any one time increased significantly. Experimentally, the growth of NCD and UNCD is often described as being controlled by renucleation processes, although exactly where the renucleation occurs is not known. From these simulations, one possibility is that instead of a defect forming at the edge of an island, maybe as a migrating species adheres incorrectly, the mismatch between grains occurs when the initial critical nucleus is formed. Two independent islands that nucleate at different locations but which are slightly misoriented with respect to each other would eventually meet and form a grain boundary. Since in NCD and UNCD growths, these critical nuclei form very often, one possibility is that slight misorientations of these, or errors with their registration to the underlying substrate, might also result in small crystal size and apparent renucleation.

Second, the number of surface layers present at any instant during growth appears to correlate with diamond quality. For SCD, only ~2-3 layers were present, effectively flat, monolayer islands were coalescing. Since all these islands were (supposedly) registered with the underlying layer, they can merge perfectly with no obvious mechanism for twinning and/or defects to occur. For MCD, the number of surface layers simultaneously present increases to 3-4, for NCD, 5-6, and for UNCD growth, the number of layers present was >6. Thus, increasingly, the situation becomes one where multilayer growth islands can meet and attempt to merge. If the upper layers of two multilevel islands were to attempt to bond before the lower ones, then not only would there be the possibility of creating voids in the lower layer but also some of the lattice registration may be lost, leading to a mismatch. We suggest this as a possible mechanism for "renucleation" or twin formation during CVD. Such a model would imply that if CVD could occur wholly layer-by-layer, then SCD would result. But the more opportunity there is for multiple layers to form at the same time, the greater the chance for these multilayer islands to meet and merge imperfectly to initiate a twin or grain boundary. This is suggested as a topic for further study by atomic-scale simulations of surface structures.

Insertion by CH_x ($x = 0$-2) species directly into the surface dimer bonds has been suggested as another growth mechanism[37] that competes with the standard model of CH_3 adsorption onto radical sites. Our simulations show that insertions are negligible for CH and CH_2 species for all deposition conditions, mainly as a result of their very low gas-phase concentrations at the surface. However, atomic C can have a significantly higher concentration above the surface, especially under SCD or MCD conditions, which results in the contribution to the growth from C insertion being ~5% and ~1% for these two conditions, respectively (Table III). Insertions do not require surface migration and are purely ER processes. Thus, there is the suggestion that such insertions may be a cause of renucleation or defect formation and thus are detrimental to the growth of good quality diamond. However, the rapid decrease of the number of C insertions in the sequence SCD-MCD-NCD-UNCD (Table III) contradicts this argument. This is an area which needs more detailed study by atomic-scale *ab initio* methods.

The critical nucleus for three dimensions is the same as that found in our 2D modelling, namely, a surface dimer consisting of 2 bonded carbon units, for all types of diamond growth. This reflects the high energy barrier needed for removal of a sidewall atom, making the size and shape of surface islands irrelevant when considering island growth.

A natural extension to this work is to replace the rigid cubic lattice with a more realistic 3D diamond lattice similar to those used by Grujicic and Lai and Netto and Frenklach in their KMC simulations. This should allow predictions of important growth features such as grain boundaries, twinning, void formation, hydrogen trapping, dislocations, and other defect formation, as well as the morphology of the crystallites and allow the KMC simulations to become a significant predictive tool.

ACKNOWLEDGMENTS

The authors would like to thank the EPSRC for funding this work under Grant No. EP/H043292/1, including a

Reuse of AIP Publishing content is subject to the terms: https://publishing.aip.org/authors/rights-and-permissions. Downloaded to IP: 134.58.253.57 On: Tue, 19 Apr 2016 09:12:27

studentship for W.J.R. P.W.M. also thanks Yuri Mankelevich for useful comments and discussions. The raw data for this paper can be accessed via the University of Bristol data repository.

[1]P. W. May, Science **319**, 1490-1491 (2008).
[2]P. W. May, Philos. Trans. R. Soc., A **358**, 473-495 (2000).
[3]D. G. Goodwin and J. E. Butler, in *Handbook of Industrial Diamonds and Diamond Films*, edited by M. A. Prelas, G. Popovici, and L. K. Bigelow (Marcel Dekker, New York, 1998).
[4]A. Cheesman, J. N. Harvey, and M. N. Ashfold, J. Phys. Chem. A **112**, 11436-11448 (2008).
[5]J. E. Butler and R. L. Woodin, Philos. Trans. R. Soc., A **342**, 209-224 (1993).
[6]S. J. Harris, Appl. Phys. Lett. **56**, 2298 (1990).
[7]K. Larsson, Phys. Rev. B **56**, 15452 (1997).
[8]D. J. Poferl, N. C. Gardner, and J. C. Angus, J. Appl. Phys. **44**, 1418 (1973).
[9]R. E. Rawles, S. F. Komarov, R. Gat, W. G. Morris, J. B. Hudson, and M. P. D'Evelyn, Diamond Relat. Mater. **6**, 791 (1997).
[10]N. Lee and A. Badzian, Diamond Relat. Mater. **6**, 130 (1997).
[11]N. Lee and A. Badzian, Appl. Phys. Lett. **66**, 2203 (1995).
[12]R. E. Stallcup II, Y. Mo, T. W. Scharf, and J. M. Perez, Diamond Relat. Mater. **16**, 1727 (2007).
[13]M. Naamoun, A. Tallaire, F. Silva, J. Achard, P. Doppelt, and A. Gicquel, Phys. Status Solidi A **209**, 1715 (2012).
[14]H. Kawarada, H. Sasaki, and A. Sato, Phys. Rev. B **52**, 11351 (1995).
[15]P. W. May and Y. A. Mankelevich, J. Phys. Chem. C **112**, 12432 (2008).
[16]A. Netto and M. Frenklach, Diamond Relat. Mater. **14**, 1630 (2005).
[17]P. W. May, N. L. Allan, J. C. Richley, M. N. R. Ashfold, and Y. A. Mankelevich, J. Phys.: Condens. Matter **21**, 364203 (2009).
[18]P. W. May, N. L. Allan, M. N. R. Ashfold, J. C. Richley, and Y. A. Mankelevich, Diamond Relat. Mater. **19**, 389 (2010).
[19]P. W. May, J. N. Harvey, N. L. Allan, J. C. Richley, and Y. A. Mankelevich, J. Appl. Phys. **108**, 014905 (2010).
[20]P. W. May, J. N. Harvey, N. L. Allan, J. C. Richley, and Y. A. Mankelevich, J. Appl. Phys. **108**, 114909 (2010).
[21]M. Grujicic and S. G. Lai, J. Mater. Sci. **34**, 7 (1999).
[22]M. Grujicic and S. G. Lai, J. Mater. Sci. **35**, 5359 (2000).
[23]M. Grujicic and S. G. Lai, J. Mater. Sci. **35**, 5371 (2000).
[24]J. C. Richley, "Fundamental studies of diamond chemical vapour deposition: Plasma diagnostics and computer modelling," Ph.D. thesis (University of Bristol, UK, 2011) available online at: http://www.chm.bris.ac.uk/pt/diamond/jamesrthesis/James-Richley-thesis.pdf.
[25]J. Achard, F. Silva, O. Brinza, X. Bonnin, V. Milne, R. Issaoui, M. Kasu, and A. Gicquel, Phys. Status Solidi A **206**, 1949 (2009).
[26]J. C. Richley, J. N. Harvey, and M. N. R. Ashfold, in *Diamond Electronics and Bioelectronics—Fundamentals to Applications III*, MRS Symposia Proceedings Vol. 1203, edited by P. Bergonzo, J. E. Butler, R. B. Jackman, K. P. Loh, and M. Nesládek, (Materials Research Society, Pittsburgh, 2010), pp. J17-J32.
[27]A. Stukowski, Modell. Simul. Mater. Sci. Eng. **18**, 015012 (2010), *Ovito* software available free from: http://www.ovito.org.
[28]P. W. May and Y. A. Mankelevich, Mater. Res. Soc. Symp. Proc. **1282** (2011).
[29]S. Skokov, B. Weiner, and M. Frenklach, J. Phys. Chem. **98**, 7073-7082 (1994).
[30]C. C. Battaile, D. J. Srolovitz, I. I. Oleinik, D. G. Pettifor, A. P. Sutton, S. J. Harris, and J. E. Butler, J. Chem. Phys. **111**, 4291-4299 (1999).
[31]W. J. Rodgers, "Multi-scale modelling of diamond grown via chemical vapour deposition," Ph.D. thesis (University of Bristol, UK, 2014).
[32]J. C. Angus and J. W. Ponton, Surf. Sci. **61**, 451 (1976).
[33]J. E. Butler and I. Oleynik, Philos. Trans. R. Soc., A **366**, 295 (2008).
[34]M. Naamoun, A. Tallaire, J. Achard, F. Silva, L. William, P. Doppelt, and A. Gicquel, Phys. Status Solidi A **210**, 1985 (2013).
[35]T. Teraji, S. Mitani, and T. Ito, Phys. Status Solidi A **198**, 395 (2003).
[36]Y. Mankelevich and P. W. May, personal communication (2015).
[37]J. C. Richley, J. N. Harvey, and M. N. R. Ashfold, J. Phys. Chem. A **113**, 11416-11422 (2009).

Reuse of AIP Publishing content is subject to the terms: https://publishing.aip.org/authors/rights-and-permissions. Downloaded to IP: 134.58.253.57 On: Tue, 19 Apr 2016 09:12:27